The density of ambient black carbon retrieved by a new method: implications to CCN prediction

Jingye Ren[1, 2], Lu Chen[1], Jieyao Liu[1], Fang Zhang[2*]

[1]*College of Global Change and Earth System Science, Beijing Normal University, Beijing 100875, China*

[2]*Shenzhen Key Laboratory of Organic Pollution Prevention and Control, School of Civil and Environmental Engineering, Harbin Institute of Technology (Shenzhen), 518055 Shenzhen, China*

***Correspondence to:* Fang Zhang (zhangfang2021@hit.edu.cn)**

Abstract.

The effective density of black carbon (BC) is a crucial factor relevant to its aging degree that would add uncertainty in evaluating its climate effect. Here, we have developed a new method to retrieve the effective density of internally mixed BC in the atmosphere combining field observations conducted from 15 November to 14 December 2016 in urban Beijing with the Köhler theory. The uncertainty of the retrieval method was evaluated within ±30 %, which was primarily caused by assumptions on both the hygroscopic parameter of organics and the proportional distribution of primary organic aerosols in different hygroscopic modes. Using the method, we obtain that the ambient internally mixed BC, accounting for 80±20 % of total BC aerosol particles, was retrieved with a campaign mean density of 1.1±0.6 g cm^{-3} during the observed periods. The retrieved result was comparable with that reported in the literature. By applying a lower (0.14 g cm^{-3}) and upper (2.1 g cm^{-3}) limit of the retrieved BC density in cloud condensation nuclei (CCN) number concentration (N_{CCN}) estimation, we derived that neglect of such variations in BC density would lead to an uncertainty of -28 %~11 % in predicting N_{CCN} at supersaturations of 0.23 % and 0.40 %. We also find that the N_{CCN} was more sensitive to the variations of BC density when it was <1.0 g cm^{-3}. This illustrates a necessity of accounting for the effect of BC density on CCN activity closer to source regions where the BC particles are mostly freshly emitted. The CCN closure achieved when introducing the retrieved real-time BC density and mixing state. This study provides a unique way of utilizing field measurements to infer ambient BC

density and highlights the importance of applying variable BC density values in models when predicting CCN and assessing its relevant climate effect.

1 Introduction

Black carbon (BC) aerosols, as the major absorber of solar radiation, play a vital role in energy budget and climate of the earth-atmosphere system by affecting the radiative forcing and cloud properties (Flanner et al., 2007; Ramanathan and Carmichael, 2008). The light-absorbing capability induced by BC is related to its density and morphology (Zhang et al., 2008; Rissler et al., 2014), which can be modified after mixing with other atmospheric aerosol particles (Khalizov et al., 2009; Xue et al., 2009). Changes in its physicochemical properties or the aging process would also regulate its ability to serve as cloud condensation nuclei (CCN) and further affect the CCN number concentrations (Zhang et al., 2016a, 2017; Ren et al., 2023) and the radiative balance by affecting the clouds process (Yuan et al., 2008; Wang et al., 2011). Owing to the complex evolution of the mixing state, density and morphology of BC, the contribution of BC particles to CCN budgets is still not well understood.

BC particles, with diesel vehicles, industrial and residential coal combustion as major sources, are ubiquitous in urban environments (Bond et al., 2013; Dameto et al., 2017; Li et al., 2017; Liu et al., 2019a). The mixing state of BC describes the distribution of the bare BC and coating masteries among the aerosol population. Typically, freshly generated BC exists in the form of chain aggregates and initially uncoated, which is known as externally mixed BC (Ex-BC). When the BC particles

were emitted, they generally mix with other materials by condensation, coagulation, and other processes (Riemer et al., 2004; Zhang et al., 2008; Liu et al., 2013; Zhang et al., 2020a), forming the internally mixed BC (In-BC) particles consisting of BC core and other chemical components (Cheng et al., 2006; Zhang et al., 2016b). The BC structure would be more compact with regular shapes (Pagels et al., 2009; Zhang et al., 2008; Wang et al., 2017), and the effective density of internally mixed BC is changed accordingly with the reconstruction (Liu et al., 2019b). The density and morphology of BC particles are closely related to its sources, mobility size, coating thickness, coating material and its chemical composition (Pagels et al., 2009; Zhang et al., 2022). A wide range of BC density has been reported in previous studies (Lide 1992; McMurry et al., 2002; Park et al., 2004; Kiselev et al., 2010). Recent field measurement has indicated that the average BC density is ~1.2 g cm^{-3} in the ambient atmosphere (Zhang et al., 2016b). Field measurements have also indicated that a considerable fraction of externally mixed/uncoated BC exists (Clarke et al., 2004; Cheng et al., 2012), although a higher proportion of internally mixed/aged BC particles in the ambient atmosphere were observed (Schwarz et al., 2008; Massoli et al., 2015; Chen et al., 2020). In climate models, the BC was generally assumed completely internally mixed and treated to have a void-free spherical structure and a density value of 1.8 g cm^{-3} (Bond et al., 2013). This may lead to bias in estimating the climate effect driven by BC.

Previous study based on a case study has shown that when the aging degree of ambient particles was low, the BC density (~1.8 g cm^{-3}) under the spherical assumption would lead to the overestimation of particle hygroscopicity by 40-50 % and the

overestimation could be explained almost 100 % using the effective density of fresh BC (~0.45 g cm^{-3}) (Fan et al. 2020). This indicates the importance of using reasonable BC density values in the calculation of particle hygroscopicity. In addition, when estimating the CCN number concentration, a significant bias of –35 % ~ +20 % was found due to the assumption of particle mixing state (Ren et al., 2018). However, these studies have not yet accounted for such impact of BC density and mixing state on CCN prediction due to lack of real time measurement data. Moreover, although the BC accounts for very small mass fractions (5~10 %) in total fine aerosols, according to our previous field observed results, the BC-containing particles could contribute 60 %-78 % toward the total number concentration in urban Beijing (Chen et al., 2020). This is comparable to the other results using SP2 instrument, which measured that the number fractions of the coated BC-containing aerosols could be as high as about 50-80 % at the field sites in north China (Liu et al., 2019b; Zhao et al., 2022). Therefore, the effect of BC density on the uncertainty of CCN prediction should be concerned carefully.

The mixing state and the density of BC particles are usually directly measured by several techniques, such as an integrated system of a volatility tandem differential mobility analyzer and a single particle soot photometer (VTDMA-SP2) (Zhang et al., 2016b), or a differential mobility analyzer with a SP2 (DMA-SP2) (Olfert et al., 2007; Rissler et al., 2014; Wu et al., 2019), and a differential mobility analyzer–centrifugal particle analyzer–single-particle soot photometer (DMA–CPMA–SP2) system (Liu et al., 2019b; Yu et al., 2020), etc. However, such techniques or measurements are not available in many previously conducted filed campaigns. In this study, we develop a

novel method for retrieving the mixing state and effective density of ambient BC particles by combining field measured hygroscopic growth factor and aerosol chemical composition and Köhler theory (Petters and Kreidenweis, 2007). The uncertainty of the new retrieval method was evaluated. The retrieved results were also compared and validated with existing observations. In addition, the effect of BC density and mixing state on prediction of CCN number concentrations was further evaluated through a sensitivity and closure test by accounting for the retrieved real-time variations of BC density and mixing state.

2 Field measurements and methodology

2.1 Field measurements

Measurements in this study were conducted from 15 November to 14 December 2016 at a typical urban site of Beijing (39.97°N, 116.37°E, 49 m above sea level). The site locates at the Institute of Atmospheric Physics, Chinese Academy of Sciences, which is mainly influenced by the surrounding cooking, road traffic and residential coal burning emissions during the home heating periods (Sun et al., 2016). The detailed information about the sampling site was presented in previous studies (Sun et al., 2016; Zhang et al., 2019). The number concentration of condensation nuclei (CN) at each size was measured by a scanning mobility particle sizer, which was equipped with a differential mobility analyzer (DMA; model 3081, TSI) and a condensation particle counter (CPC; model 3772, TSI). Subsequently, the mono-dispersed particles were introduced into a Droplet Measurement Technologies CCN counter (CCNc, DMT;

Lance et al., 2006) to measure CCN number concentration. A hygroscopic tandem differential mobility analyzer (HTDMA) system was used to measure the hygroscopic growth factor (Gf) (Tan et al., 2013). Here, four diameters of 40, 80, 110, 150, and 200 nm were selected in the campaign. Gf is defined as the ratio of the mobility diameter at the given RH to the dry diameter (Petters and Kreidenweis, 2007). The nonrefractory submicron aerosol chemical composition was measured by an Aerodyne high-resolution time-of-flight aerosol mass spectrometer (HR-AMS; Xu et al., 2019), including sulfate, nitrate, ammonium, chloride, and organics. Two factors, including a non-hygroscopic primary organic aerosol (POA) and hygroscopic secondary organic aerosol (SOA) were classified by positive matrix factorization (PMF) with PMF algorithm (v4.2) method (Paatero and Tapper, 1994) and followed the procedures reported in Ulbrich et al. (2009). The refractory black carbon mass loading was measured by an aethalometer (model AE33, Magee Scientific Corporation). Both the nonrefractory materials and BC mass concentration were measured with diameters < 1.0 μm. The detailed description of the instrument operation and data process have been described in details elsewhere (Ren et al., 2018; Xu et al., 2019; Zhang et al., 2019; Fan et al., 2020).

2.2 Retrieving the mixing state and density of BC

2.2.1 Retrieving the mixing state of BC

The Gf probability distribution function (Gf-PDF) for a specified diameter can be retrieved firstly based on the TDMAinv algorithm (Gysel et al., 2009). The κ-PDF can

be further calculated based on the Gf-PDF (Fan et al., 2020). Size-resolved κ is derived using κ-Köhler theory based on hygroscopic growth factor (Gf) (Petters and Kreidenweis, 2007),

$$\kappa_{gf} = (\mathrm{Gf}^3 - 1) \cdot \left[\frac{1}{\mathrm{RH}} \exp\left(\frac{4\sigma_{s/a} M_w}{RT\rho_w D_d \mathrm{Gf}}\right) - 1\right] \quad (1)$$

where Gf is hygroscopic growth factor, RH is the relative humidity in the HTDMA (90 %), D_d is the dry diameter, $\sigma_{s/a}$ is assumed to be the surface tension of pure water, R is the universal gas constant, T is the temperature, M_w and ρ_w is the molecular mass, and the density of water, respectively.

The κ-PDF patterns of particles in different sizes always present two modes: nearly hydrophobic (NH) mode with $\kappa_{gf} \leqslant 0.1$ and more hygroscopic (MH) mode with $\kappa_{gf} > 0.1$ (Fig. S1). Firstly, based on the κ-PDF patterns, the number fraction (NF) of the total nearly hydrophobic group with the boundary of [0, 0.1] was calculated according to the following equation:

$$NF = \int_0^{0.1} c(\kappa, D_p)\, d\kappa \quad (2)$$

here, the κ-PDF, represented by c (κ, D_p), was normalized as $\int c(\kappa, D_p)\, d\kappa = 1$, where κ can be replaced by κ_{gf}, D_p is the selected electrical mobility diameter in the campaign.

The nearly hydrophobic mode consists of both externally mixed POA (Ex-POA or bare POA) and externally mixed BC (Ex-BC). Since the number fraction of the nearly-hydrophobic POA would change with the emission and aging processes, in this study, we have applied different values for the number fractions of hydrophobic POA (NH-POA) under clean (91 %), moderately polluted (70 %), and heavily polluted conditions

(31 %) by referring to the literature (Liu et al., 2021a), as shown in Fig. S2. The number concentration of Ex-BC was then calculated using the total number fraction of NH mode minus the number of NH-POA.

$$N_{POA-containing} = N_{total} \times NF_{POA-containing}$$

$$N_{bare-POA} = N_{POA-containing} \times NF_{bare-POA}$$

$$N_{Ex-BC} = N_{NH} - N_{bare-POA} \quad (3)$$

where $N_{\text{POA-containing}}$ and $NF_{\text{POA-containing}}$ are the number concentration and fraction of POA-containing particles, N_{total} is the total number concentration, $N_{\text{bare-POA}}$ and $NF_{\text{bare-POA}}$ are the number concentration and fraction of bare POA particles, and N_{NH} is the number of nearly hydrophobic group.

The number size distribution of the externally mixed BC ($n_{\text{Ex-BC}}$ (log D_{p})) can be calculated based on the particle number size distribution (PNSD) and the number fraction of the hydrophobic mode of BC ($NF_{\text{Ex-BC}}$) as follows:

$$n_{\text{Ex-BC}}(\log D\text{p}) = NF_{\text{Ex-BC}} \times n\ (\log D\text{p}) \quad (4)$$

where n (log D_{p}) is the function of the aerosol number size distribution, D_{p} is the mobility diameter.

By assuming that the particles were spherical (Rader and McMurry, 1986), the mass size distribution of Ex-BC ($M_{\text{Ex-BC}}$) was obtained as follows:

$$M_{\text{Ex-BC}}(\log D\text{p}) = \frac{\pi}{6} {D_p}^3 \rho n_{\text{Ex-BC}}(\log D\text{p}) \quad (5)$$

where D_{p} is the mobility diameter, ρ is the effective density of Ex-BC, and $n_{\text{Ex-BC}}$ (log D_{p}) is the function of the number size distribution of Ex-BC, respectively. By reviewing and summarizing the existing results, we show that typical values of density for the

196 freshly emitted or externally mixed BC observed in the winter of urban Beijing or North
197 China Plain span over 0.14-0.50 g cm^{-3}, with a mean of ~0.40±0.10 g cm^{-3} (Fig. S3), in
198 the size range of 100 to 300 nm, where the mass concentration of externally mixed BC
199 mostly concentrated (Geller et al., 2006; Wu et al., 2019; Liu et al., 2020; Zhao et al.,
200 2022). Therefore, an average $\rho_{\text{Ex-BC}}$ of 0.4 g cm^{-3} was used for calculating the mass
201 concentration of externally mixed BC in our study. Uncertainty analyses due to the
202 variations of $\rho_{\text{Ex-BC}}$ were given in section 2.3.

203 The mass size distribution of Ex-BC was fit using the log-normal distribution as
204 shown in Fig. S4 (Wu et al., 2017; Liu et al., 2019a; Zhao et al., 2022). Thus, the bulk
205 mass concentration of Ex-BC can be calculated from the integration of the mass size
206 distribution:

207 $$m_{\text{Ex-BC}} = \int_{D_{start}}^{D_{end}} M_{\text{Ex-BC}}(\log D_p)\ d\log(D_p) \quad (6)$$

208 $$m_{\text{In-BC}} = m_{\text{BC}} - m_{\text{Ex-BC}} \quad (7)$$

209 where D_{start} and D_{end} are the lower and upper size limit, $M_{\text{Ex-BC}}$ (log D_{p}) is the function
210 of the Ex-BC mass size distribution. We then obtained the bulk mass concentration of
211 internally mixed BC ($m_{\text{In-BC}}$) by subtracting $m_{\text{Ex-BC}}$ from the bulk BC mass
212 concentration measured by AE33 in equation (7). It should be noted that the mass
213 concentration of BC obtained from AE33 based on aerosol light absorption may lead
214 some uncertainties, as has been further addressed in section 2.3.

215 2.2.2 Retrieving the density of BC

216 For retrieval of the density of BC, the principal idea is to use the measured κ_{gf} to

calculate the density of BC based on the Zdanovskii–Stokes–Robinson (ZSR) mixing rule (Stokes and Robinson, 1966; Zdanovskii, 1948) with the chemical composition measured by AMS (Petters & Kreidenweis, 2007). In the retrieval, several aspects are concerned. First, since the ZSR rule assumes the aerosol particles are internally mixed, the κ_{gf} value of the more MH mode ($\kappa_{gf\text{-}MH}$) is thus applied for retrieving the density of internally mixed BC. Second, since the size distribution of BC number concentration is usually with peaks between 100 and 200 nm (Liu et al., 2019a; Yu et al., 2020; Zhao et al., 2022), the $\kappa_{gf\text{-}MH}$ value of particles in accumulation mode was averaged and applied for the retrieval. Previous studies showed an independence of $\kappa_{gf\text{-}MH}$ on particle size when the D_p >100 nm during the campaign period (Fan et al., 2020). Therefore, the average of $\kappa_{gf\text{-}MH}$ in accumulation mode is reasonable for the determination of the In-BC density. Third, since only one hydrophobic and/or one hygroscopic mode was observed by the HTDMA in most cases during the campaign (Fig. S1, S5), the chemical components of the more hygroscopic (MH) mode at a given diameter should contain both these hygroscopic non-BC and the coatings on BC-containing particles, which would be measured by the HR-AMS instrument together. Therefore, by subtracting the externally mixed POA in non-hygroscopic mode (see section 2.3), the concentration and mass fraction of each component measured by HR-AMS can represent the overall chemical composition of MH modes, and thus was applied in the ZSR mixing rule for the retrieval of the density of internally mixed BC in this study. In addition, because the inversion including measurements from HTDMA and HR-AMS, a total mass closure of the measured aerosol particles was conducted between the two techniques by

comparing the mass concentration of PM_1 and the results are well consistent (Fig. S6). The density of internally mixed BC (In-BC), $\rho_{\text{In-BC}}$ is then derived from the following equations:

$$\kappa_{gf-MH} = \kappa_{chem} = \sum_i \varepsilon_i \kappa_i = \frac{v_{inorg}}{v_{total}}\kappa_{inorg} + \frac{v_{SOA}}{v_{total}}\kappa_{SOA} + \frac{v_{In-POA}}{v_{total}}\kappa_{POA} + \frac{v_{In-BC}}{v_{total}}\kappa_{BC} \quad (8)$$

where $\kappa_{\text{gf-MH}}$ is the hygroscopic parameter of the more hygroscopic (MH) mode, κ_{chem} is the hygroscopic parameter of aerosol particles in the mixed composition and can be calculated based on chemical volume fractions using a simple rule (Stokes and Robinson, 1966; Petters & Kreidenweis, 2007), κ_i is the hygroscopic parameter of each pure composition and ε_i is the volume faction of the individual components in the internally mixed particle. v_{inorg}, v_{SOA} and $v_{\text{In-POA}}$ are the volume of the inorganic, SOA and internally mixed POA species, and can be calculated as follows: $v_{inorg} = \frac{m_{inorg}}{\rho_{inorg}}$, $v_{SOA} = \frac{m_{SOA}}{\rho_{SOA}}$, and $v_{In-POA} = \frac{m_{In-POA}}{\rho_{POA}}$. v_{total} is the total volume of all the species and can be written as $v_{total} = \frac{m_{inorg}}{\rho_{inorg}} + \frac{m_{SOA}}{\rho_{SOA}} + \frac{m_{In-POA}}{\rho_{POA}} + \frac{m_{In-BC}}{\rho_{In-BC}}$. In equation (8), κ_{BC} and κ_{POA} are assumed to be 0. So, the total volume v_{total} can be further written as $v_{total} = \frac{v_{inorg}\kappa_{inorg} + v_{SOA}\kappa_{SOA}}{\kappa_{gf-MH}}$. The volume of internally mixed $v_{\text{In-BC}}$ can be calculated as follows,

$$v_{In-BC} = \frac{v_{inorg}\kappa_{inorg} + v_{SOA}\kappa_{SOA}}{\kappa_{gf-MH}} - v_{inorg} - v_{SOA} - v_{In-POA}$$
$$= \frac{\frac{m_{inorg}}{\rho_{inorg}}\kappa_{inorg} + \frac{m_{SOA}}{\rho_{SOA}}\kappa_{SOA}}{\kappa_{gf-MH}} - \frac{m_{inorg}}{\rho_{inorg}} - \frac{m_{SOA}}{\rho_{SOA}} - \frac{m_{In-POA}}{\rho_{POA}} \quad (9)$$

then, the $\rho_{\text{In-BC}}$ can be calculated based on its mass concentration and volume as follows:

$$\rho_{In-BC} = \frac{m_{In-BC}}{\left(\frac{\frac{m_{inorg}}{\rho_{inorg}}\kappa_{inorg} + \frac{m_{SOA}}{\rho_{SOA}}\kappa_{SOA}}{\kappa_{gf-MH}} - \frac{m_{inorg}}{\rho_{inorg}} - \frac{m_{SOA}}{\rho_{SOA}} - \frac{m_{In-POA}}{\rho_{POA}}\right)} \quad (10)$$

where, $m_{\text{In-BC}}$ is the mass concentration of internally mixed BC, m_{inorg} and m_{SOA} are the mass concentrations of the inorganic species and SOA, which are measured by the AMS. $m_{\text{In-POA}}$ is the mass concentrations of internally mixed POA and can be calculated

through subtracting the mass fraction of NH-POA from the total mass concentrations of POA. ρ_{inorg}, ρ_{SOA} and ρ_{POA} are the density of the inorganic species, SOA and POA. Since the AMS measures the concentrations of the organic and inorganic ions, including SO_4^{2-}, NO_3^-, NH_4^+, Cl^-. Here inorganic species were derived by applying a simplified ion pairing scheme (Gysel et al., 2007) to convert mass concentrations of ions to the inorganic salts as follows:

$$n_{NH_4NO_3} = n_{NO_3^-}$$

$$n_{NH_4HSO_4} = \min(2n_{SO_4^{2-}} - n_{NH_4^+} + n_{NO_3^-}, n_{NH_4^+} - n_{NO_3^-})$$

$$n_{(NH_4)_2SO_4} = \max(n_{NH_4^+} - n_{NO_3^-} - n_{SO_4^{2-}}, 0)$$

$$n_{H_2SO_4} = \max(0, n_{SO_4^{2-}} - n_{NH_4^+} + n_{NO_3^-}) \quad (11)$$

where *n* represents the number of moles, and the mass concentrations were obtained by the number of moles times the molar mass of each inorganic salts. Because the value of the $n_{H_2SO_4}$ was zero in this campaign. Three inorganic salts including NH_4HSO_4, $(NH_4)_2SO_4$, and NH_4NO_3 were applied in our study. The densities for inorganic salts were taken from previous studies (Gysel et al., 2007; Wu et al., 2016). Here the densities for three inorganics are 1.78, 1.77 and 1.72 g cm^{-3}, respectively. By summarizing the previous studies (Gysel et al., 2007; Dinar et al., 2006), 1.4 g cm^{-3} was selected as the density of SOA (ρ_{SOA}). The density of POA (ρ_{POA}) is assumed to be 1.0 g cm^{-3} for urban environments, which is similar to the that of the lubricating oil (Wu et al., 2016). Since the cooking organic aerosols represent a high contribution to POA in urban environments, we choose the mean density of the rapeseed oil and oleic acid (~0.85 g cm^{-3}) (Reyes-Villegas et al., 2018) to evaluated the result as shown in section 2.3. The

values of κ for inorganic components are 0.56 for NH_4HSO_4, 0.48 for $(NH_4)_2SO_4$ and 0.58 for NH_4NO_3, along with the best-fit values for the three inorganic salts (Petters & Kreidenweis, 2007 and Gunthe et al., 2009). The κ_{SOA} is assumed to be 0.15 according to the field studies in urban areas (Chang et al., 2010; Kawana et al., 2016).

Note that the method fails to retrieve the BC density when organic accounts for a large fraction (>60 %). This is because that a higher fraction of OA usually corresponds to lower total volume of all the species (Fig. S7), yielding negative values for $v_{In\text{-}BC}$ introduced in equation (9). As a result, 61 % of the data observed during the campaign were valid for calculating the BC density.

Similarly, the bulk density of BC ($\rho_{bulk\text{-}BC}$) is calculated with the same method as that for calculating the $\rho_{In\text{-}BC.}$ When calculating the $\rho_{bulk\text{-}BC}$, the bulk κ_{gf} value measured by HTDMA is applied assuming that all the aerosol particles are internally mixed.

2.3 Uncertainties and limitations

For the retrieval, the assumptions on the values of κ_{SOA}, ρ_{POA}, ρ_{SOA} and $\rho_{Ex\text{-}BC}$ as well as the fraction of primary organic aerosols in non-hygroscopic mode would add uncertainty in the inferred values of ambient internally mixed BC density. For example, the freshly emitted POA particles might consistently be coated with secondary particles during the aging process, resulting in changes of the $NF_{NH\text{-}POA}$. However, a real-time variation of the $NF_{NH\text{-}POA}$ is not yet available due to the lack of such measurement data.

Applying only rough fractions of hydrophobic POA for three different atmospheric conditions could still cause uncertainties. Also, the densities of POA and

SOA may differ due to their precursors, emission sources and the formation mechanisms in ambient atmosphere (Alfarra et al., 2006; Reyes-Villegas et al., 2018). The density of Ex-BC is generally characterized by the morphology and size (Wu et al., 2019). In addition, the value of κ_{SOA} spans largely due to the variations in the emissions of gas precursors and formation processes under different atmospheric conditions (Zhang et al., 2015; Liu et al., 2021b). Therefore, we examined the sensitivities of In-BC density to the variations of these factors, as exhibited in Fig. 1 and Fig. 2.

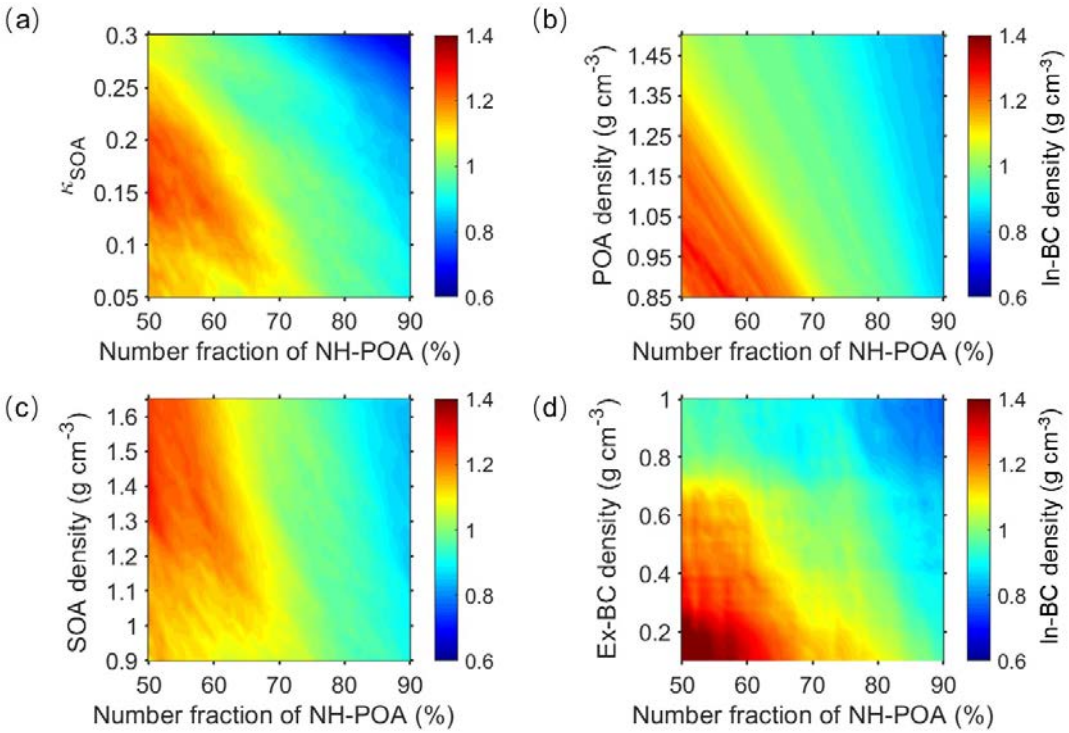

Figure 1. Sensitivities of In-BC density to the variations in the number fraction of nearly hydrophobic (NH) POA and hygroscopic parameter of OA (k_{SOA}) (a), POA density (b), SOA density (c) and the externally mixed BC density (d).

The figures show that the In-BC density gradually decreased with the increment of the $NF_{NH\text{-}POA}$, implying the high fraction of bare POA particles corresponded to the early aging stage of aerosol particles. With the increase of κ_{SOA}, the In-BC density was

generally reduced, but with small fluctuations (Fig. 1a, Fig. 2b). This suggests a complex impact of assumptions of κ_{SOA} on the retrieved BC density. In addition, the In-BC density decreased slightly as $\rho_{Ex\text{-}BC}$ increased (Fig. 2e), suggesting applying a larger $\rho_{Ex\text{-}BC}$ would derive smaller values for In-BC density. The In-BC density was insensitive to the changes of the density of POA and SOA, showing an almost negligible effect on the retrieved results (Fig. 2c and d).

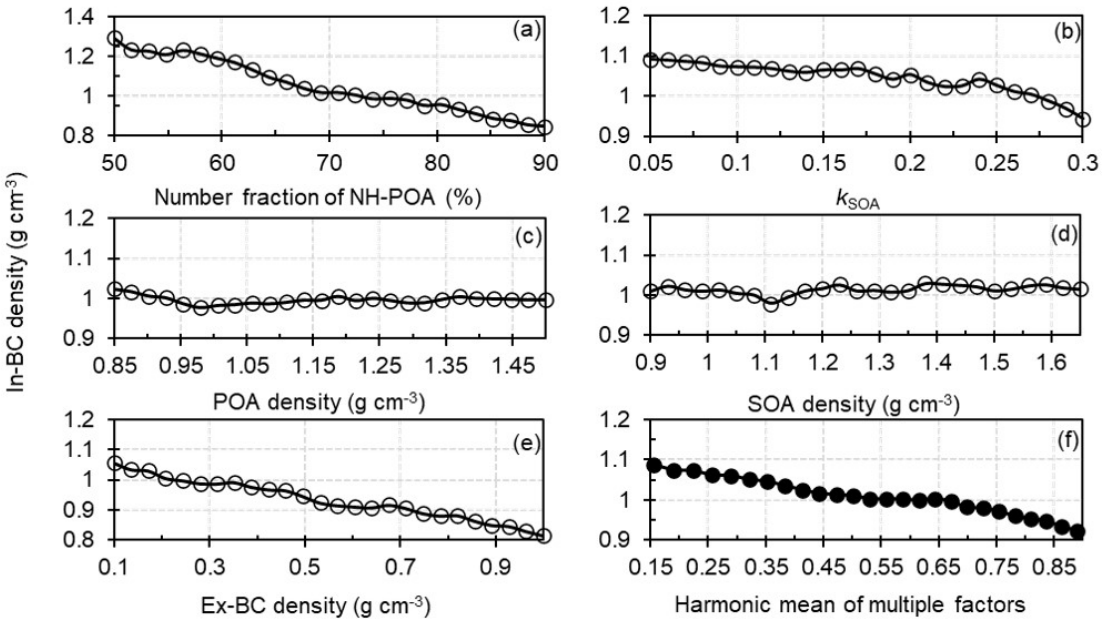

Figure 2. Sensitivity of the In-BC density to variations in the number fraction of nearly hydrophobic (NH) POA (a), the hygroscopic parameter of SOA (b), the POA density (c), the SOA density (d), the externally mixed BC density (e) and the harmonic mean of multiple factors (f).

The uncertainty analysis shows that, by comparing the results based on the mean fraction of the $NF_{NH\text{-}POA}$ with a typical atmospheric observed range of 50-90 % for the $NF_{NH\text{-}POA}$ (Liu et al., 2021a), the assumption on $NF_{NH\text{-}POA}$ can lead to relative deviations (uncertainty) of -17 %~+27 % for the retrieved BC density (Fig. 3a).

In addition, unlike inorganics (eg., NH_4HSO_4, $(NH_4)_2SO_4$ and NH_4NO_3), for which the hygroscopicity has been already well-understood (Petters and Kreidenweis, 2007), the hygroscopicity of organic species varies largely due to the complexity in organic aerosol constituents. Therefore, the assumption of the values of κ_{SOA} will add the uncertainty in the calculation of BC density. Previous studies have suggested that the organics have a wide range of κ values ranging from 0.05 to 0.3 (Jimenez et al., 2009; Mei et al., 2013). Thus, the sensitivity test has also been done to examine the effect due to changes in κ_{SOA} on calculating the density of BC (Fig. 1a). The result shows that the assumption of κ_{SOA} values can cause an average relative deviation of -10 %~+3 % in calculating the density of In-BC (Fig. 3b).

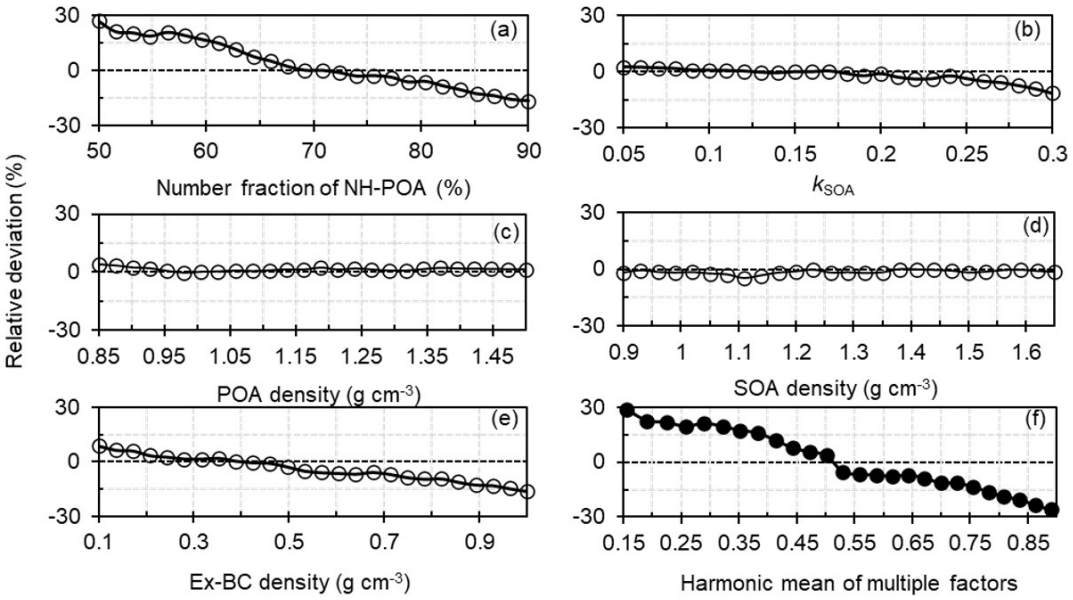

Figure 3. Relative deviations of the number fraction of nearly hydrophobic (NH) POA to the In-BC density (a), the hygroscopic parameter of OA to the In-BC density (b), the POA density to the In-BC density (c), the SOA density to the In-BC density (d), the externally mixed BC density to In-BC density (e) and the combined deviations based

on multiple factors mentioned above (f).

However, the sensitivity test shows that the impact of both the ρ_{POA} and ρ_{SOA} variations on the BC density estimation was very small or even negligible (Fig. 1b, c). By varying the ρ_{POA} from 0.85 to 1.5 g cm^{-3} and the ρ_{SOA} from 0.9 to 1.65 g cm^{-3} according to the literature (Noureddini et al., 1992; Alfarra et al., 2006; Reyes-Villegas et al., 2018; Kostenidou et al., 2007), the retrieval uncertainties in the BC density were both within ±5 % (Fig. 3c, d). For $\rho_{Ex\text{-}BC}$, it exhibited that the evolution of the $\rho_{Ex\text{-}BC}$ could lead to an average deviation of -16 %~+9 % in calculating In-BC density (Fig. 3e) when increasing the values of $\rho_{Ex\text{-}BC}$ from 0.1 to 1.0 g cm^{-3}, which represents a typical range in ambient atmosphere (Wu et al., 2019; Liu et al., 2020). A combined uncertainty (δ) caused by the multiple factors (δ_i), which was calculated by equation (12), was -26 %~+29 % as shown in Fig. 3f.

$$\delta = \sqrt{\sum_{i=1}^{n} {\delta_i}^2} \quad (12)$$

In addition, it should be noted that the mass concentration of BC obtained from AE33 based on aerosol light absorption may lead some uncertainties. However, the comparison of the simultaneously measured data by SP2 with those by AE33 during the campaign shows that the temporal variations of BC mass concentrations measured by the two techniques were well consistent (Fig. S8). Note that the BC mass measured by SP2 is occasionally low probably because of the low detection efficiency in small size (McMeeking et al., 2010; Schwarz et al., 2006). In addition, the SP2 is unable to quantify the BC mass beyond a certain limit because of the saturation of electronic devices recording signals (Pileci et al., 2021). We show that, compared the results that

were retrieved if applying the BC mass measured by SP2, the BC density retrieved based on AE33 can be 18 % higher. Given the measurement bias from SP2, this overestimation indicates an upper limit of the uncertainty.

3 Results and Discussion

3.1 A comparison and validation of retrieved mixing state and density of BC

Figure 4a shows retrieved time series of the mixing state of ambient BC during the campaign. Large temporal variations of the mass fraction of internally and externally mixed BC present during the observed period at the sites. The temporal changes should be related to the atmospheric aging process or diurnal variations of emissions (Liu et al., 2019a; Fan et al., 2020). Statistically, the average mass fractions of externally and internally mixed BC were 20±18 % and 80±20 % respectively, showing that most of the BC particles were aged and internally mixed with other components. Previous studies at urban sites have shown the co-existence of the externally mixed BC in the ambient atmosphere (Schwarz et al., 2008; Cheng et al., 2012; Chen et al., 2020) due to continuous combustion processes (e.g., vehicle exhaust and residential sector) (Wang et al., 2017; Liu et al., 2019a). Our results are basically comparable with those previously reported results, which are directly measured or indirectly retrieved. For example, Chen et al. (2020) found that the mass fraction of internally mixed BC particles was nearly ~80–90 % in summer of Beijing based on VTDMA measurements. Liu et al. (2020) using a tandem system with an aerodynamic aerosol classifier and SP2, reported that the mass fraction of internally BC-containing particles would increase

with increasing size and reach ~70 % in Beijing. Overall, the mass fraction obtained in our study was comparable with that reported in urban Beijing. Previous studies also displayed that the significant diversity of the BC mixing state among emission conditions and coating processes (Shiraiwa et al., 2008; Pan et al., 2017; Zhang et al., 2020b). Accordingly, the densities of the bulk and internally mixed BC present apparent fluctuations as shown in Fig. 4b, which is significantly affected by the variations of BC emission sources and BC aging processes. The density of the In-BC during daytime was

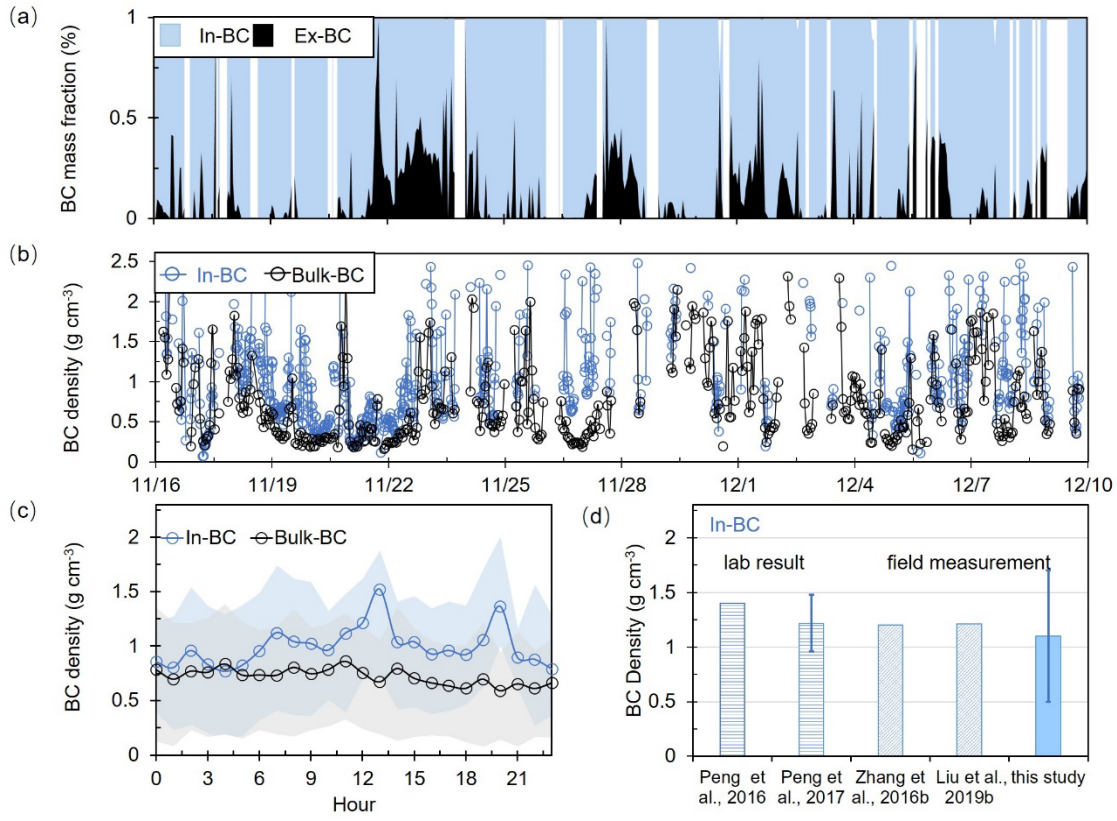

Figure 4. (a) Time series of the mass fraction of the retrieved internal- and external-mixed BC; (b) Time series of the retrieved density of the bulk and internal- mixed BC (In-BC); (c) Diurnal variation of the retrieved density of bulk and In-BC; (d) Comparison of the results of the derived In-BC density in this study with that reported in the literature.

generally higher than that at night (Fig. 4c). The elevated BC density during daytime was likely due to the strong photochemical processes promote the aging of BC particles, which resulted in a conversion from uncompacted structure to compact and regular spherical shapes of BC (Qiao et al., 2018; Liu et al., 2019b). The rising in BC density around 20:00 LT might indicate that the BC particles would be rapidly coated with secondary inorganic aerosol (SIA) particles and continuously aged in the polluted period due to the heterogeneous reactions of SIA in urban regions (Zhang et al., 2016b; Peng et al., 2017). Actually, following the haze evolution, the fraction of nearly hydrophobic group reduced rapidly (Fig. S9). Consequently, the average density of In-BC increased obviously from the clean conditions to the polluted periods (Fig. S5). A slight decrease was observed in the bulk BC density during traffic hours. This is likely associated with the continuous emissions (e.g., vehicle exhaust) that lead to uncoated or uncompacted BC particles in this period. The diurnal cycle in In-BC density was consistent with the coating thickness measured by a tandem CPMA-SP2-DMA-SP2 (Liu et al., 2020), demonstrating that the new method can derive the density of ambient BC particles reasonably. Averagely, the campaign average values of the bulk and internally mixed BC densities were 0.7±0.5 and 1.1±0.6 g cm^{-3} respectively, which were much less than 1.8 g cm^{-3}, implying that the BC particles are not void-free spheres in the urban atmosphere. The results of In-BC density were comparable with those observed at other sites in North China Plain (NCP) as shown in Fig. 4d, illustrating that the BC effective density retrieved by this method was within the range of density from field measurements.

Based on both field measurements (e.g., Lide 1992; Zhang et al., 2016b; Wu et al., 2019; Liu et al., 2019b) and laboratory studies (e.g., McMurry et al., 2002; Park et al., 2003, 2004; Olfert et al., 2007; Kiselev et al., 2010; Gysel et al., 2011, 2012), the BC density from diverse combustion sources or representing different aging degree has

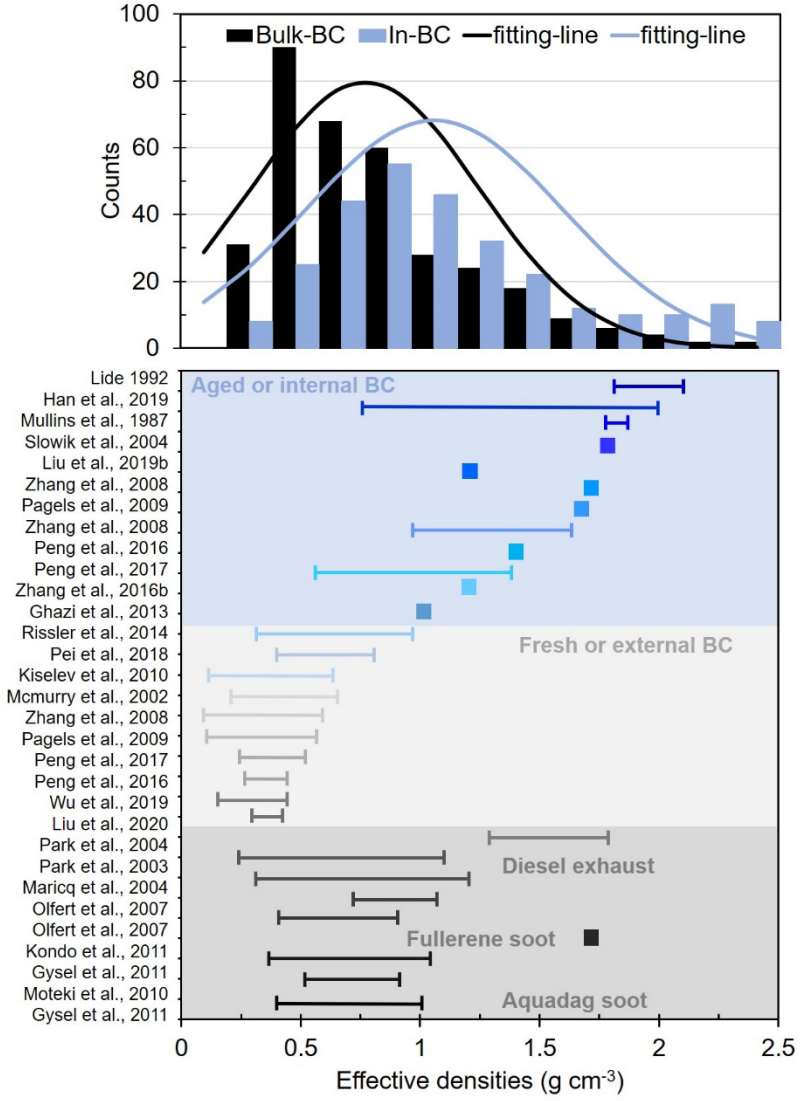

Figure 5. The probability distribution function (PDF) of the retrieved density of bulk and In-BC and the measured density distribution spectrum of BC from different sources reported in the literature.

been obtained and ranges widely from 0.14 to 2.1 g cm^{-3}, as was summarized and shown in Fig. 5. Mean probability distribution function (PDF) of the density of bulk and In-

436 BC retrieved by this study is also presented in Fig. 5. It shows that the retrieved density
437 of bulk BC exhibited a dominant mode with a peak value at 0.7 g cm^{-3}, which was
438 situated between the typical density range of those externally mixed and internally
439 mixed BC measured previously. For the In-BC, the PDF was with a peak value at 1.1 g
440 cm^{-3}, but ranged widely from ~0.5 to 2.5 g cm^{-3}, which indicated various morphologies,
441 different aging degree and compositions of ambient BC particles due to the complex
442 impact of multiple local sources and aging processes during the observed period in
443 urban Beijing. Overall, the retrieved values for In-BC density fall within the range of
444 typical internally mixed BC reported in the literature, verifying the reliability of our
445 inversion results.

446 **3.2 Sensitivity of predicted N_{CCN} to changes of BC density**

447 A previous study showed that the use of an inaccurate density value of BC particles
448 would result in large biases in estimating κ of ambient aerosol particles with the ZSR
449 mixing rule (Fan et al., 2020), as would further lead to uncertainties in prediction of
450 N_{CCN} and relevant climate effects. Considering the large variation range of BC density
451 during the campaign, which is closely associated with BC morphology or degree of BC
452 aging, we further examine the sensitivity of critical supersaturation (S_c), critical
453 diameter (D_{cut}) and predicted N_{CCN} to variations of BC density (Fig. 6). Here, we use
454 the critical diameter and particle number size distribution to calculate N_{CCN}. The method
455 to derive the critical diameter is based on Köhler theory and ZSR rule. Three CCN
456 closure studies were assumed to evaluate the effect of BC density and mixing state on

prediction of CCN number concentrations. Closure studies provide a useful way to

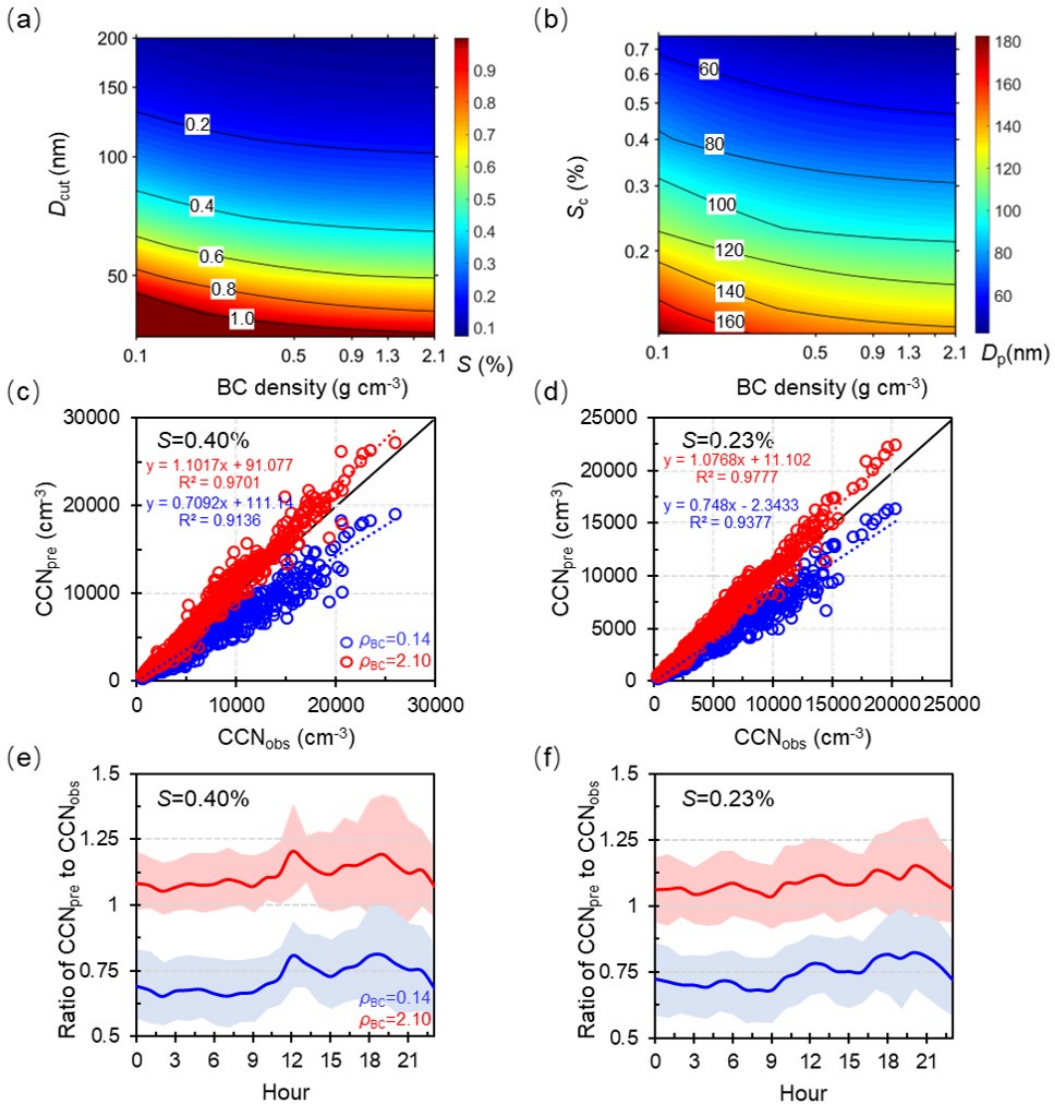

Figure 6. Sensitivity of critical supersaturation (S_c) (a) and diameter (D_{cut}) (b) to the variations in BC density; Predicted N_{CCN} as a function of measured N_{CCN} by varying the density from 0.14 to 2.1 g cm^{-3} at S=0.40 % (c) and S=0.23 % (d), the black solid line is the 1:1 line; Diurnal variations in the ratio of predicted-to-measured N_{CCN} at S=0.40 % (e) and S=0.23 % (f).

investigate the importance of aerosol properties to CCN concentration prediction. If the closure study is achieved, it means the bias between the predicted and measured CCN concentrations is within ±15 % (Chang et al., 2007). The detailed calculation methods

are presented in the supporting information (SI: Methods) or the reference in Ren et al. (2018). The results show that, by varying the value of density from 0.14 to 2.1 g cm^{-3} that represents the range of BC density in the atmosphere, the D_{cut} reduced apparently at a given supersaturation (S) (Fig. 6a), or similarly, the S_c decreased rapidly for a given particle size (Fig. 6b). The results show that the changes of the D_{cut} and S_c were more sensitive when the BC density was below 1.0 g cm^{-3}. The effects on the D_{cut} and S_c both gradually weakened with the increase of BC density. This shows that it is critical to apply more accurate BC density for the aerosol particles with low aging degree in predicting CCN and its climate effect. Accordingly, the ratios of predicted-to-measured N_{CCN} ranged from 0.72 to 1.11 by varying the BC density from 0.14 to 2.1 g cm^{-3} at the typical S of 0.23 % and 0.40 % (Fig. 6c, 6d), showing an estimation uncertainty of -28 % ~ 11 % in N_{CCN} prediction.

The diurnal variations in the ratio of predicted-to-measured N_{CCN} at S=0.40 % and 0.23 % are shown to examine the response of the BC density on N_{CCN} prediction at different time periods (Fig. 6e, 6f). By applying the lower limit of density value of 0.14 g cm^{-3}, the prediction was much worse than the use of the density of 2.1 g cm^{-3} at night (00:00-06:00 LT), when the latter was much closer to the real density of ambient BC (Fig. 4c). The prediction was improved substantially by applying the value of 0.14 g cm^{-3} during evening rush hours (18:00-20:00 LT), during which the ambient BC particles were disturbed by the traffic emissions (Fig. 4c). The prediction became worse by applying the value of 2.1 g cm^{-3} and an obvious overestimation by up to ~40 % was shown. The results further illustrate that it is critical to account for the real-time mixing

state and density of BC particles in N_{CCN} prediction, particularly in regions with heavy traffic and residential coal emissions.

It should be noted that the assumption of the surface tension of water would overestimate the critical diameter and underpredict CCN number concentration. While the surface tension depression might be more obvious for the small size particles (<60 nm), as the fraction of organics is higher at small particles size (Meng et al., 2014; Cai et al., 2018). Here, in this study, we calculated the critical diameters at supersaturations of 0.40 % and 0.23 %, typical values in cloud, corresponding to larger sizes (> 70 nm and 90 nm) of aerosols. Therefore, the uncertainties from the application of the surface tension of pure water should be negligible (< 10 %).

3.3 N_{CCN} prediction based on the real-time variations of BC density and mixing state

Figure 7 exhibits the comparisons between predicted and measured N_{CCN} at S of 0.23 % and 0.40 % by accounting for the retrieved real-time variations of BC density and mixing state. It shows that the N_{CCN} can be well predicted with a slope of 1.01 and 1.02 at S of 0.23 % and 0.40 % respectively (Fig. 7a, 7b), only presenting a slight deviation. The slight deviation is primarily due to the fixed value of the density for the externally mixed BC caused by the retrieved method, especially during noontime and evening rush periods (Fig. 7c and 7d).

The diurnal variations in the ratio of predicted-to-measured N_{CCN} shows the N_{CCN} can be underestimated by up to 15 % at S=0.40 % during noontime. While, a slightly overrated during the evening traffic hours and nighttime may be due to the

underestimation of the number fraction of Ex-BC. Overall, the dependence of the CCN prediction on S is due to the size dependence of κ and mixing state (Zhang et al., 2017; Liu et al., 2020; Ren et al., 2018). A better closure at S=0.23 % is because the bulk κ of particles is closer to that at the critical diameter of 100-150 nm. Similarly, the effect on CCN prediction induced by the bulk mixing state would be more critical for smaller particles, corresponding to the critical diameter at high S.

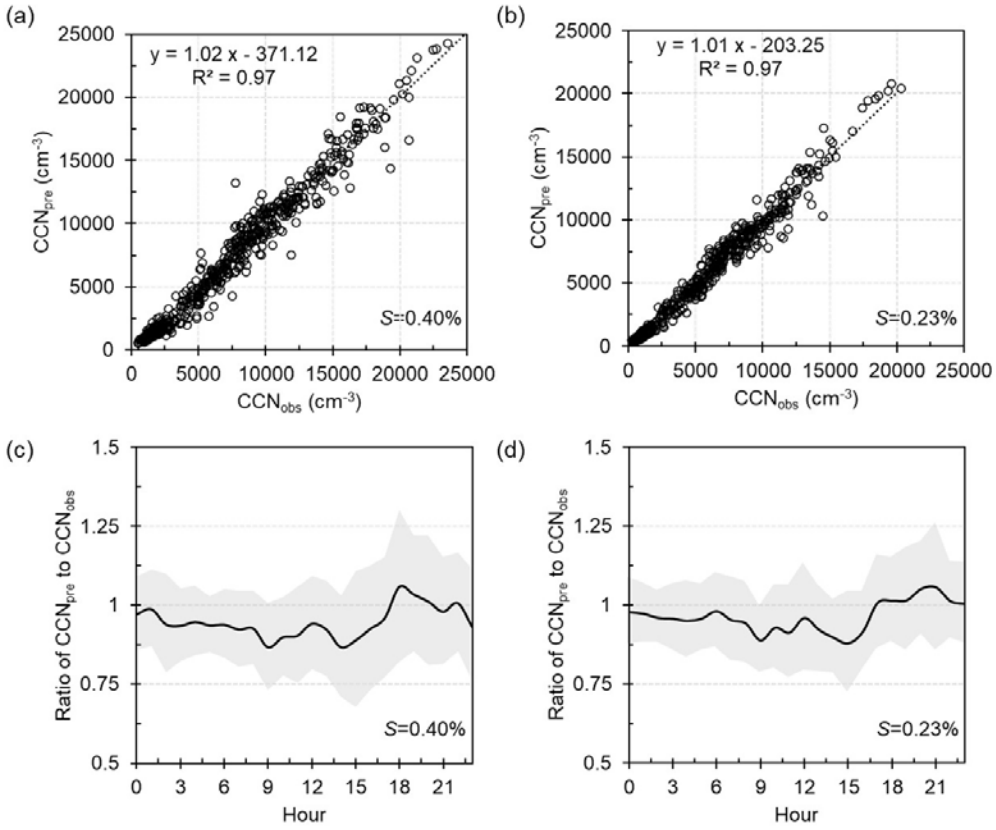

Figure 7. Predicted CCN number concentration using the mixing state and In-BC density derived from HTDMAs at S=0.40 % (a) and S=0.23 % (b). Diurnal variations in the ratio of predicted-to-measured N_{CCN} at S=0.40 % (c) and S=0.23 % (d).

Overall, when considering the effective density of BC relevant to its mixing state, the CCN closure achieves. Previous studies have shown that the fresh emitted BC particles may convert from fractal-like aggregates to a compact structure and its density

would increase with the aging process (Liu et al., 2019b; Zhang et al., 2020a, 2022), but the actual density of In-BC may be lower than 1.8 g cm^{-3} in the ambient atmosphere according to this study. Therefore, the currently applied value represents a density of the void-free structure of BC particles may cause an overestimation in CCN prediction. In addition, although the BC accounts for small mass fractions in ambient fine aerosols, according to the measurements simultaneously conducted at the site, the BC-containing particles could contribute 60 %-78 % toward the total number concentration in urban Beijing (Chen et al., 2020). Our results further highlight the effect of BC density on the uncertainty of CCN prediction should be concerned carefully.

4 Conclusions

The mixing state and effective density of BC changed through heterogenous chemistry process and thus would cause uncertainty in evaluating its CCN activity. In this study, we develop a new method to retrieve the mixing state and effective density of ambient BC using field measurements and the Köhler theory. The uncertainty of the new retrieval method was evaluated within ±30 %, which was primarily caused by assuming the value of κ_{SOA} and the fraction of primary organic aerosols in non-hygroscopic mode. The retrieved results show that most of the BC particles were aged and internally mixed with other components, with mean mass fraction of 80±20 %. Averagely, the retrieved densities of the bulk and internally mixed BC were 0.7±0.5 and 1.1±0.6 g cm^{-3} respectively, but ranged widely from ~0.1 to 2.5 g cm^{-3}, indicating various morphologies, different aging degree and compositions of ambient BC particles

due to the complex impact of multiple local sources and aging processes during the observed period. The retrieved result was basically comparable with previous observations in North China Plain.

Further examination shows the uncertainties of the N_{CCN} prediction were -28 % ~11 % at the typical S of 0.23 % and 0.40 % by varying the BC density from 0.14 to 2.1 g cm^{-3} that represented the range of ambient BC particles. Moreover, the prediction was found more sensitive to the variations of BC density when it was <1.0 g cm^{-3}, suggesting a great significance of accounting for the effect of BC density for the aerosol particles with low aging degree when evaluating the climate effect. The CCN closure achieved when introducing the retrieved real-time BC density relevant to its mixing state. This work provides a unique way of utilizing field observations to infer ambient BC density and highlights the current assumption of a void-free structure of BC particles in models would cause large uncertainties in CCN prediction and in the relevant climate effect evaluation.

The method used to derive the ambient BC density has limitations. Since the assumptions on the values of κ_{SOA}, ρ_{POA}, ρ_{SOA} and $\rho_{Ex\text{-}BC}$ as well as the fraction of primary organic aerosols in non-hygroscopic mode would add uncertainty in the inferred values of ambient internally mixed BC density. It is thus necessary to examine observational data to verify this methodology in future studies. However, the method and results of this study could provide the way for a more comprehensive understanding of the variations in BC density in Beijing. Additionally, it has the potential to reveal the uncertainties of usage of void-free structure of BC density in assessing the climate

effects.

Data availability.

All data needed to evaluate the conclusions in the paper are present in the paper and/or the Supplement. All data used in the study are also available from the corresponding author upon request (zhangfang2021@hit.edu.cn).

Author contributions.

FZ and JR conceived the conceptual development of the manuscript. JR directed and performed of the experiments with JL, LC, and FZ. JR conducted the data analysis and wrote the draft of the manuscript. All authors edited and commented on the various sections of the manuscript.

Acknowledgments.

This work was funded by the National Natural Science Foundation of China (NSFC) research project (41975174, 41675141), Shenzhen Science and Technology Plan Project (Grant No. GXWD20220811174022002). We thank all participants in the field campaigns for their tireless work and cooperation. We also thank Dr. Yele Sun and his group for providing the data of nonrefractory submicron aerosol chemical composition.

Competing interests.

The contact author has declared that neither they nor their co-authors have any competing interests.

References

Alfarra, M. R., Paulsen, D., Gysel, M., Garforth, A. A., Dommen, J., Prévôt, A. S. H., Worsnop, D. R., Baltensperger, U., and Coe, H.: A mass spectrometric study of secondary organic aerosols formed from the photooxidation of anthropogenic and biogenic precursors in a reaction chamber, Atmos. Chem. Phys., 6, 5279– 5293, https://doi:10.5194/acp-6-5279-2006, 2006.

Bond, T. C., Doherty, S. J., Fahey, D., Forster, P., Berntsen, T., DeAngelo, B., Flanner, M., Ghan, S., Kärcher, B., and Koch, D.: Bounding the role of black carbon in the climate system: A scientific assessment, J. Geophys. Res.-Atmos., 118(11), 5380–5552, https://doi.org/10.1002/jgrd.50171, 2013

Cheng, Y. F., Eichler, H., Wiedensohler, A., Heintzenberg, J., Zhang, Y. H., Hu, M., Herrmann, H., Zeng, L. M., Liu, S., Gnauk, T., Brüggemann, E., and He, L. Y.: Mixing state of elemental carbon and non-light-absorbing aerosol components derived from in situ particle optical properties at Xinken in Pearl River Delta of China, J. Geophys. Res., 111, D20204, doi:10.1029/2005JD006929, 2006.

Clarke, A.D., Shinozuka, Y., Kapustin, V.N., Howell, S., Huebert, B., Doherty, S., Anderson, T., Covert, D., Anderson, J., Hua, X., Moore II, K.G., McNaughton, C., Carmichael, G., Weber, R.: Size distributions and mixtures of dust and black carbon aerosol in Asian outflow: physiochemistry and optical properties, J. Geophys. Res.-Atmos., 109, D15S09, https://doi.org/10.1029/2003JD004378, 2004.

Cheng, Y. F., Su, H., Rose, D., Gunthe, S. S., Berghof, M., Wehner, B., Achtert, P., Nowak, A., Takegawa, N., Kondo, Y., Shiraiwa, M., Gong, Y. G., Shao, M., Hu, M., Zhu, T., Zhang, Y. H., Carmichael, G. R., Wiedensohler, A., Andreae, M. O., and Pöschl, U.: Size-resolved measurement of the mixing state of soot in the megacity Beijing, China: diurnal cycle, aging and parameterization, Atmos. Chem. Phys., 12, 4477–4491, https://doi.org/10.5194/acp-12-4477-2012, 2012.

Chen, L., F. Zhang, P. Yan, X. Wang, L. Sun, Y. Li, X. Zhang, Y. Sun, and Z. Li.: The large proportion of black carbon (BC)-containing aerosols in the urban atmosphere, Environ. Pollut., 263, 114507, https://doi.org/10.1016/j.envpol.2020.114507, 2020.

Chang, R. Y.-W., Slowik, J. G., Shantz, N. C., Vlasenko, A., Liggio, J., Sjostedt, S. J., Leaitch, W. R., and Abbatt, J. P. D.: The hygroscopicity parameter (κ) of ambient organic aerosol at a field site subject to biogenic and anthropogenic influences: relationship to degree of aerosol oxidation, Atmos. Chem. Phys., 10, 5047–5064,

https://doi:10.5194/acp-10-5047-2010, 2010.
Chang, R. Y. W., Liu, P. S. K., Leaitch, W. R., and Abbatt, J. P. D.: Comparison between measured and predicted CCN concentrations at Egbert, Ontario: Focus on the organic aerosol fraction at a semirural site, Atmos. Environ., 41, 8172–8182, https://doi:10.1016/j.atmosenv.2007.06.039, 2007.
Cai, M., Tan, H., Chan, C. K., Qin, Y., Xu, H., Li, F., Schurman, M. I., Liu, L., and Zhao, J.: The size-resolved cloud condensation nuclei (CCN) activity and its prediction based on aerosol hygroscopicity and composition in the Pearl Delta River (PRD) region during wintertime 2014, Atmos. Chem. Phys., 18, 16419–16437, https://doi.org/10.5194/acp-18-16419-2018, 2018.
Dameto de España, C., Wonaschütz, A., Steiner, G., Rosati, B., Demattio, A., Schuh, H., and Hitzenberger, R.: Long-term quantitative field study of New Particle Formation (NPF) events as a source of Cloud Condensation Nuclei (CCN) in the urban background of Vienna, Atmos. Environ., 164, 289–298, https://doi.org/10.1016/j.atmosenv.2017.06.001, 2017.
Dinar, E., Mentel, T. F., and Rudich, Y.: The density of humic acids and humic like substances (HULIS) from fresh and aged wood burning and pollution aerosol particles, Atmos. Chem. Phys., 6, 5213–5224, doi:10.5194/acp-6-5213-2006, 2006.
Flanner, M. G., Zender, C. S., Randerson, J. T., and Rasch, P. J.: Present-day climate forcing and response from black carbon in snow, J. Geophys. Res.-Atmos., 112, D11202, https://doi.org/10.1029/2006JD008003, 2007.
Fan, X., Liu, J., Zhang, F., Chen, L., Conllins, D., Xu, W., Jin, X., Ren, J., Wang, Y.,Wu, H., Li, S., Sun, Y., Li, Z.: Contrasting size-resolved hygroscopicity of fine particles derived by HTDMA and HR-ToF-AMS measurements between summer and winter in Beijing: the impacts of aerosol aging and local emissions, Atmos. Chem. Phys. 20, 915-929, https://doi.org/10.5194/acp-20-915-2020, 2020.
Gysel, M., McFiggans, G. B., and Coe, H.: Inversion of tandem differential mobility analyser (TDMA) measurements, J. Aerosol Sci., 40, 134–151, https://doi.org/10.1016/j.jaerosci.2008.07.013, 2009.
Geller, M., Biswas, S., and Sioutas, C.: Determination of particle effective density in urban environments with a differential mobility analyzer and aerosol particle mass analyzer, Aerosol Sci. Technol., 40, 709–723, https://doi.org/10.1080/02786820600803925, 2006.
Gysel, M., Crosier, J., Topping, D. O., Whitehead, J. D., Bower, K. N., Cubison, M. J., Williams, P. I., Flynn, M. J., McFiggans, G. B., and Coe, H.: Closure study between chemical composition and hygroscopic growth of aerosol particles during TORCH2, Atmos. Chem. Phys., 7, 6131–6144, https://doi.org/10.5194/acp-7-6131-2007, 2007.
Gunthe, S. S., King, S. M., Rose, D., Chen, Q., Roldin, P., Farmer, D. K., Jimenez, J. L., Artaxo, P., Andreae, M. O., Martin, S. T., and Pöschl, U.: Cloud condensation nuclei in pristine tropical rainforest air of Amazonia: size resolved measurements and modeling of atmospheric aerosol composition and CCN activity, Atmos. Chem. Phys., 9, 7551–7575, https://doi.org/10.5194/acp-9-7551-2009, 2009.
Gysel, M., Laborde, M., Olfert, J. S., Subramanian, R., & Gröhn, A. J.: Effective density of aquadag and fullerene soot black carbon reference materials used for SP2

663 calibration, Atmos. Meas. Tech., 4(12), 4937–4955, https://doi.org/10.5194/amt-4-
664 2851-2011, 2011.
665 Gysel, M., Laborde, M., Mensah, A. A., Corbin, J. C., Keller, A., Kim, J., et al.:
666 Technical note: The single particle soot photometer fails to reliably detect PALAS
667 soot nanoparticles, Atmos. Meas. Tech., 5(12), 3099–3107,
668 https://doi.org/10.5194/amt-5-3099-2012, 2012.
669 Jimenez, J. L., Canagaratna, M. R., Donahue, N. M., Prevot, A. S. H., Zhang, Q., Kroll,
670 J. H., DeCarlo, P. F., Allan, J. D., Coe, H., Ng, N. L., Aiken, A. C., Docherty, K. S.,
671 Ulbrich, I. M., Grieshop, A. P., Robinson, A. L., Duplissy, J., Smith, J. D., Wilson,
672 K. R., Lanz, V. A., Hueglin, C., Sun, Y. L., Tian, J., Laaksonen, A., Raatikainen, T.,
673 Rautiainen, J., Vaattovaara, P., Ehn, M., Kulmala, M., Tomlinson, J. M., Collins, D.
674 R., Cubison, M. J., Dunlea, E. J., Huffman, J. A., Onasch, T. B., Alfarra, M. R.,
675 Williams, P. I., Bower, K., Kondo, Y., Schneider, J., Drewnick, F., Borrmann, S.,
676 Weimer, S., Demerjian, K., Salcedo, D., Cottrell, L., Griffin, R., Takami, A., Miyoshi,
677 T., Hatakeyama, S., Shimono, A., Sun, J. Y., Zhang, Y. M., Dzepina, K., Kimmel, J.
678 R., Sueper, D., Jayne, J. T., Herndon, S. C., Trimborn, A. M., Williams, L. R., Wood,
679 E. C., Middlebrook, A. M., Kolb, C. E., Baltensperger, U., and Worsnop, D. R.:
680 Evolution of Organic Aerosols in the Atmosphere, Science., 326, 1525–1529,
681 https://doi.org/10.1126/science.1180353, 2009.
682 Khalizov, A. F., Zhang, R., Zhang, D., Xue, H., Pagels, J., and McMurry, P. H.:
683 Formation of highly hygroscopic soot aerosols upon internal mixing with sulfuric
684 acid vapor, J. Geophys. Res.-Atmos., 114, D05208,
685 https://doi.org/10.1029/2008jd010595, 2009.
686 Kiselev, A., Wennrich, C., Stratmann, F., Wex, H., Henning, S., Mentel, T.F., Kiendler-
687 Scharr, A., Schneider, J., Walter, S., Lieberwirth, I.: Morphological characterization
688 of soot aerosol particles during LACIS Experiment in November (LExNo), J.
689 Geophys. Res. -Atmos., 115, D11204. https://doi.org/10.1029/2009jd012635, 2010.
690 Kawana, K., Nakayama, T., and Mochida, M.: Hygroscopicity and CCN activity of
691 atmospheric aerosol particles and their relation to organics: Characteristics of urban
692 aerosols in Nagoya, Japan, J. Geophys. Res.-Atmos., 121, 4100–4121,
693 https://doi.org/10.1002/2015JD023213, 2016.
694 Kostenidou, E., Pathak, R. K., & Pandis, S. N.: An Algorithm for the Calculation of
695 Secondary Organic Aerosol Density Combining AMS and SMPS Data, Aerosol
696 Science and Technology, 41:11, 1002-1010, https://doi:
697 10.1080/02786820701666270, 2007.
698 Li, M., Zhang, Q., Kurokawa, J.-I., Woo, J.-H., He, K., Lu, Z., Ohara, T., Song, Y.,
699 Streets, D. G., Carmichael, G. R., Cheng, Y., Hong, C., Huo, H., Jiang, X., Kang, S.,
700 Liu, F., Su, H., and Zheng, B.: MIX: a mosaic Asian anthropogenic emission
701 inventory under the international collaboration framework of the MICS-Asia and
702 HTAP, Atmos. Chem. Phys., 17, 935–963, https://doi.org/10.5194/acp-17-935-2017,
703 2017.
704 Liu, D., Joshi, R., Wang, J., Yu, C., Allan, J. D., Coe, H., Flynn, M. J., Xie, C., Lee, J.,
705 Squires, F., Kotthaus, S., Grimmond, S., Ge, X., Sun, Y., and Fu, P.: Contrasting
706 physical properties of black carbon in urban Beijing between winter and summer,

Atmos. Chem. Phys., 19, 6749–6769, https://doi.org/10.5194/acp-19-6749-2019, 2019a.
Liu, D., Allan, J., Whitehead, J., Young, D., Flynn, M., Coe, H., McFiggans, G., Fleming, Z. L., and Bandy, B.: Ambient black carbon particle hygroscopic properties controlled by mixing state and composition, Atmos. Chem. Phys., *13*, 2015–2029, https://doi.org/10.5194/acp-13-2015-2013, 2013.
Liu, H., Pan, X.L., Wu, Y., Wang, D.W., Tian, Y., Liu, X.Y., et al.: Effective densities of soot particles and their relationships with the mixing state at an urban site in the Beijing megacity in the winter of 2018, Atmos. Chem. Phys. 19, 14791–14804, https://doi.org/10.5194/acp-19-14791-2019, 2019b.
Lide, D. R. (ed.). CRC Handbook of Chemistry and Physics. CRC Press: Ann Arbor, MI. (1992).
Lance, S., Medina, J., Smith, J., and Nenes, A.: Mapping the operation of the DMT continuous flow CCN counter, Aerosol Sci. Tech., 40, 242–254, https://doi.org/10.1080/02786820500543290, 2006.
Liu, L, Zhang, J, Zhang, Y, Wang, Y, Xu, L, Yuan, Q, et al.: Persistent residential burning-related primary organic particles during wintertime hazes in North China: insights into their aging and optical changes, Atmos. Chem. Phys. *21*, 2251–2265, https://doi.org/10.5194/acp-21-2251-2021, 2021a.
Liu, H., Pan, X., Liu, D., Liu, X., Chen, X., Tian, Y., Sun, Y., Fu, P., and Wang, Z.: Mixing characteristics of refractory black carbon aerosols at an urban site in Beijing, Atmos. Chem. Phys., 20, 5771–5785, https://doi.org/10.5194/acp-20-5771-2020, 2020.
Liu, J., Zhang, F., Xu, W., Sun, Y., Chen, L., Li, S.: Hygroscopicity of organic aerosols linked to formation mechanisms, Geophysical Research Letters, 48, e2020GL091683, https://doi.org/10.1029/2020gl091683, 2021b.
McMurry, H. Peter, Wang Xin, Park Kihong & Ehara Kensei.: The Relationship between Mass and Mobility for Atmospheric Particles: A New Technique for Measuring Particle Density, Aerosol Sci. Technol., 36:2, 227-238, https://doi.10.1080/027868202753504083, 2002.
Massoli, P., Onasch, T.B., Cappa, C.D., Nuamaan, I., Hakala, J., Hayden, K., Li, S.M., Sueper, D.T., Bates, T.S., Quinn, P.K., Jayne, J.T., Worsnop, D.R.: Characterization of black carbon-containing particles from soot particle aerosol mass spectrometer measurements on the R/V Atlantis during CalNex 2010, J. Geophys. Res.- Atmos., 120, 2575-2593, https://doi.org/10.1002/2014JD022834, 2015.
Mei, F., Setyan, A., Zhang, Q., and Wang, J.: CCN activity of organic aerosols observed downwind of urban emissions during CARES, Atmos. Chem. Phys., 13, 12155–12169, https://doi.org/10.5194/acp-13-12155-2013, 2013.
McMeeking, G.R., Hamburger, T., Liu, D., Flynn, M., Morgan, W.T., Northway, M., Highwood, E.J., Krejci, R., Allan, J.D., Minikin, A., Coe, H.: Black carbon measurements in the boundary layer over western and northern Europe. Atmos. Chem. Phys. 10, 9393-9414, https://doi.org/10.5194/acp-10-9393-2010, 2010.
Meng, J. W., Yeung, M. C., Li, Y. J., Lee, B. Y. L., and Chan, C. K.: Size-resolved cloud condensation nuclei (CCN) activity and closure analysis at the HKUST Supersite in

751 Hong Kong, Atmos. Chem. Phys., 14, 10267–10282, https://doi.org/10.5194/acp-14-
752 10267-2014, 2014.
753 Noureddini, H., Teoh, B. C., Davis Clements, L.: Densities of vegetable oils and fatty
754 acids, J. Am. Oil Chem. Soc., 69 (12), 1184−1188, 1992.
755 Olfert, J. S., Symonds, J. P. R., and Collings, N.: The effective density and fractal
756 dimension of particles emitted from a light-duty diesel vehicle with a diesel oxidation
757 catalyst, J. Aerosol Sci., 38, 69–82, https://doi.org/10.1016/j.jaerosci.2006.10.002,
758 2007.
759 Pagels, J., Khalizov, A.F., McMurry, P.H. and Zhang, R.Y.: Processing of soot by
760 controlled sulphuric acid and water condensation-mass and mobility relationship,
761 Aerosol Sci. Technol., 43, 629–640, https://doi.org/10.1080/02786820902810685,
762 2009.
763 Park, K., Kittelson, D. B., and McMurry, P. H.: Structural properties of diesel exhaust
764 particles measured by transmission electron microscopy (TEM): Relationships to
765 particle mass and mobility, Aerosol Sci. Technol., 38, 881–889,
766 https://doi.org/10.1080/027868290505189, 2004.
767 Petters, M. D. and Kreidenweis, S. M.: A single parameter representation of
768 hygroscopic growth and cloud condensation nucleus activity, Atmos. Chem. Phys.,
769 7, 1961–1971, https://doi.org/10.5194/acp-7-1961-2007, 2007.
770 Paatero, P. and Tapper, U.: Positive matrix factorization: A nonnegative factormodel
771 with optimal utilization of error estimates of data values, Environmetrics, 5, 111–126,
772 1994.
773 Pileci, R. E., Modini, R. L., Bertò, M., Yuan, J., Corbin, J. C., Marinoni, A., Henzing,
774 B., Moerman, M. M., Putaud, J. P., Spindler, G., Wehner, B., Müller, T., Tuch, T.,
775 Trentini, A., Zanatta, M., Baltensperger, U., and Gysel-Beer, M.: Comparison of co-
776 located refractory black carbon (rBC) and elemental carbon (EC) mass concentration
777 measurements during field campaigns at several European sites, Atmos. Meas. Tech.,
778 14, 1379–1403, https://doi.org/10.5194/amt-14-1379-2021, 2021.
779 Peng, J. F., Hu, M., Guo, S., Du, Z. F., Zheng, J., Shang, D. J., Zamora, M., Zeng, L.
780 M., Shao, M., Wu, Y. S., Zheng, J., Wang, Y., Glen, C., Collins, D., Molina, M., and
781 Zhang, R. Y.: Markedly enhanced absorption, and direct radiative forcing of black
782 carbon under polluted urban environments, P. Natl. Acad. Sci. USA, 113(16), 4266–
783 4271, https://doi.org/10.1073/pnas.1602310113, 2016.
784 Peng, J. F., Hu, M., Guo, S., Du, Z. F., Zheng, J., M., Zeng, L. M., Shao, M., Wu, Y. S.,
785 Collins, D., Molina, M., and Zhang, R. Y.: Ageing and hygroscopicity variation of
786 black carbon particles in Beijing measured by a quasi-atmospheric aerosol evolution
787 study (QUALITY) chamber, Atmos. Chem. Phys., 17(17), 10333-10348,
788 https://doi.org/10.5194/acp-17-10333-2017, 2017.
789 Pan, X.L., Kanaya, Y., Taketani, F., Miyakawa, T., Inomata, S., Komazaki, Y., et al.:
790 Emission characteristics of refractory black carbon aerosols from fresh biomass
791 burning: a perspective from laboratory experiments, Atmos. Chem. Phys., 17(21),
792 13001–13016, https://doi.org/10.5194/acp-17-13001-2017, 2017.
793 Park, K., Cao, F., Kittelson, D. B., & McMurry, P. H.: Relationship between particle

mass and mobility for diesel exhaust particles, Environ. Sci. Tehnol., 37, 577–583, https://doi.org/10.1021/es025960v, 2003.
Qiao, K., Wu, Z., Pei, X., Liu, Q., Shang, D., Zheng, J., Du, Z., Zhu,W.,Wu, Y., Lou, S., Guo, S., Chan, C.K., Pathak, R.K., Hallquist, M., Hu, M.: Size-resolved effective density of submicron particles during summertime in the rural atmosphere of Beijing. China, J. Environ. Sci. (China) 73, 69–77. https://doi.org/10.1016/j.jes.2018.01.012, 2018.
Rissler, J., Nordin, E. Z., Eriksson, A. C., Nilsson, P. T., Frosch, M., Sporre, M. K., Wierzbicka, A., Svenningsson, B., Londahl, J., Messing, M. E., Sjogren, S., Hemmingsen, J. G., Loft, S., Pagels, J. H., and Swietlicki, E.: Effective Density and Mixing State of Aerosol Particles in a Near-Traffic Urban Environment, Environ. Sci. Technol., 48, 6300–6308, https://doi.org/10.1021/es5000353, 2014.
Riemer, N., Vogel, H., and Vogel, B.: Soot aging time scales in polluted regions during day and night, Atmos. Chem. Phys., 4, 1885–1893, https://doi.org/10.5194/acp-4-1885-2004, 2004.
Ramanathan, V. and Carmichael, G.: Global and regional climate changes due to black carbon, Nat. Geosci., 36, 221-227, https://doi.org/10.1038/ngeo156, 2008.
Ren J, Zhang F, Chen L, et al.: Identifying the hygroscopic properties of fine aerosol particles from diverse sources in urban atmosphere and the applicability in prediction of cloud nuclei, Atmospheric Environment, 298: 119615, https://doi.org/10.1016/j.atmosenv.2023.119615, 2023.
Ren, J., Zhang, F., Wang, Y., Collins, D., Fan, X., Jin, X., et al.: Using different assumptions of aerosol mixing state and chemical composition to predict CCN concentrations based on field measurements in urban Beijing, Atmos. Chem. Phys., 18, 6907–6921, https://doi.org/10.5194/acp-18-6907-2018, 2018.
Rader, D.J., McMurry, P.H.: Application of the tandem differential mobility analyzer to studies of droplet growth or evaporation, J. Geophys. Res.- Atmos., 17, 771-787, https://doi.org/10.1016/0021-8502(86)90031-5, 1986.
Reyes-Villegas, E., Bannan, T., Le Breton, M., Mehra, A., Priestley, M., Percival, C., Coe, H., and Allan, J. D.: Online Chemical Characterization of Food-Cooking Organic Aerosols: Implications for Source Apportionment, Environ. Sci. Technol., 52, 5308–5318, https://doi.org/10.1021/acs.est.7b06278, 2018.
Schwarz, J. P., Gao, R. S., Spackman, J. R., Watts, L. A., Thomson, D. S., Fahey, D. W., Ryerson, T. B., Peischl, J., Holloway, J. S., Trainer, M., Frost, G. J., Baynard, T., Lack, D. A., de Gouw, J. A., Warneke, C., and Del Negro, L. A.: Measurement of the mixing state, mass, and optical size of individual black carbon particles in urban and biomass burning emissions, Geophys. Res. Lett., 35, L13810, https://doi.org/10.1029/2008GL033968, 2008.
Sun, Y., Du, W., Fu, P., Wang, Q., Li, J., Ge, X., Zhang, Q., Zhu, C., Ren, L., Xu, W., Zhao, J., Han, T., Worsnop, D. R., and Wang, Z.: Primary, and secondary aerosols in Beijing in winter: sources, variations, and processes, Atmos. Chem. Phys., 16, 8309–8329, https://doi.org/10.5194/acp-16-8309-2016,2016.
Stokes, R. and Robinson, R.: Interactions in aqueous nonelectrolyte solutions, I. Solute-solvent equilibria, J. Phys. Chem.-US, 70, 2126–2131, 1966.

Schwarz, J.P., Gao, R.S., Fahey, D.W., Thomson, D.S., Watts, L.A., Wilson, J.C., Reeves, J.M., Darbeheshti, M., Baumgardner, D.G., Kok, G.L., Chung, S.H., Schulz, M., Hendricks, J., Lauer, A., K€ archer, B., Slowik, J.G., Rosenlof, K.H., Thompson, T.L., Langford, A.O., Loewenstein, M., Aikin, K.C.: Single-particle measurements of midlatitude black carbon and light-scattering aerosols from the boundary layer to the lower stratosphere. J. Geophys. Res.: Atmosphere 111, D16207, https://doi.org/10.1029/2006JD007076, 2006.

Shiraiwa, M., Kondo, Y., Moteki, N., Takegawa, N., Sahu, L., Takami, A., et al.: Radiative impact of mixing state of black carbon aerosol in Asian outflow, J. Geophys. Res.- Atmos., 113, D24210, https://doi.org/ 10.1029/2008JD010546, 2008.

Tan, H., Xu, H., Wan, Q., Li, F., Deng, X., Chan, P. W., Xia, D., and Yin, Y.: Design and application of an unattended multifunctional H-TDMA system, J. Atmos. Ocean. Tech., 30, 1136–1148, https://doi.org/10.1175/JTECH-D-12-00129.1, 2013.

Ulbrich, I. M., Canagaratna, M. R., Zhang, Q., Worsnop, D. R., and Jimenez, J. L.: Interpretation of organic components from Positive Matrix Factorization of aerosol mass spectrometric data, Atmos. Chem. Phys., 9, 2891–2918, https://doi.org/10.5194/acp-9- 2891-2009, 2009.

Wang, Y., Wan, Q., Meng, W., Liao, F., Tan, H., and Zhang, R.: Long-term impacts of aerosols on precipitation and lightning over the Pearl River Delta megacity area in China, Atmos. Chem. Phys., 11, 12421–12436, https://doi.org/10.5194/acp-11-12421-2011, 2011.

Wang, Y. Y., Liu, F. S., He, C. L., Bi, L., Cheng, T. H., Wang, Z. L., Zhang, H., Zhang, X. Y., Shi, Z. B., and Li, W. J.: Fractal dimensions and mixing structures of soot particles during atmospheric processing, Environ. Sci. Tech. Lett., 4, 487–493, https://doi.org/10.1021/acs.estlett.7b00418, 2017.

Wu, Y. F., Xia, Y. J., Huang, R. J., Deng, Z. Z., Tian, P., Xia, X. G., et al.: A study of the morphology and effective density of externally mixed black carbon aerosols in ambient air using a size-resolved single-particle soot photometer (SP2), Atmos. Meas. Tech., 12, 4347–4359, https://doi.org/10.5194/amt-12-4347-2019, 2019.

Wu, Y., Wang, X., Tao, J., Huang, R., Tian, P., Cao, J., Zhang, L., Ho, K.-F., Han, Z., and Zhang, R.: Size distribution and source of black carbon aerosol in urban Beijing during winter haze episodes, Atmos. Chem. Phys., 17, 7965–7975, https://doi.org/10.5194/acp-17-7965-2017, 2017.

Wu, Z. J., Zheng, J., Shang, D. J., Du, Z. F., Wu, Y. S., Zeng, L. M., Wiedensohler, A., and Hu, M.: Particle hygroscopicity and its link to chemical composition in the urban atmosphere of Beijing, China, during summertime, Atmos. Chem. Phys., 16, 1123–1138, https://doi.org/10.5194/acp-16-1123-2016, 2016.

Xue, H., Khalizov, A. F., Wang, L., Zheng, J., and Zhang, R.: Effects of dicarboxylic acid coating on the optical properties of soot, Phys. Chem. Chem. Phys., 11, 7869–7875, https://doi.org/10.1039/b904129j, 2009.

Xu, W., Sun, Y., Wang, Q., Zhao, J., Wang, J., Ge, X., et al.: Changes in aerosol chemistry from 2014 to 2016 in winter in beijing: Insights from high-resolution aerosol mass spectrometry, J. Geophys. Res.-Atmos., 124, 1132–1147. https://doi.org/10.1029/2018jd029245, 2019.

Yuan, T., Li, Z., Zhang, R., and Fan, J.: Increase of cloud droplet size with aerosol optical depth: An observation and modeling study, J. Geophys. Res.-Atmos., 113, D04201, https://doi.org/10.1029/2007JD008632, 2008.

Yu, C., Liu, D., Broda, K., Joshi, R., Olfert, J., Sun, Y., Fu, P., Coe, H., Allan, J.D.: Characterising mass-resolved mixing state of black carbon in Beijing using a morphology-independent measurement method, Atmos. Chem. Phys., 20, 3645–3661. https://doi.org/10.5194/acp-20-3645-2020, 2020.

Zhang, R. Y., Khalizov, A. F., Pagels, J., Zhang, D., Xue, H. X., and McMurry, P. H.: Variability in morphology, hygroscopicity, and optical properties of soot aerosols during atmospheric processing, P. Natl. Acad. Sci. USA, 105, 10291–10296, https://doi.org/10.1073/pnas.0804860105, 2008.

Zhang, F., Li, Z., Li, Y., Sun, Y., Wang, Z., Li, P., Sun, L., Wang, P., Cribb, M., Zhao, C., Fan, T., Yang, X., and Wang, Q.: Impacts of organic aerosols and its oxidation level on CCN activity from measurement at a suburban site in China, Atmos. Chem. Phys., 16, 5413–5425, https://doi.org/10.5194/acp-16- 5413-2016, 2016a.

Zhang, F., Wang, Y., Peng, J., Ren, J., Collins, D., Zhang, R., et al.: Uncertainty in predicting CCN activity of aged and primary aerosols, J. Geophys. Res.-Atmos., 122(21), 11723–11736, https://doi.org/10.1002/2017jd027058, 2017.

Zhang, F., Wang, Y., Peng, J., Chen, L., Sun, Y., Duan, L., Ge, X., Li, Y., Zhao, J., Liu, C., Zhang, X., Zhang, G., Pan, Y., Wang, Y., Zhang, A. L., Ji, Y., Wang, G., Hu, M., Molina, M. J., Zhang, R.: An unexpected catalyst dominates formation and radiative forcing of regional haze, P. Natl. Acad. Sci. USA, 117(8), 3960-3966, https://doi.org/10.1073/pnas.1919343117, 2020a.

Zhang, Y., Zhang, Q., Cheng, Y., Su, H., Kecorius, S., Wang, Z., Wu, Z., Hu, M., Zhu, T., Wiedensohler, A., and He, K.: Measuring the morphology and density of internally mixed black carbon with SP2 and VTDMA: new insight into the absorption enhancement of black carbon in the atmosphere, Atmos. Meas. Tech., 9, 1833–1843, https://doi.org/10.5194/amt-9-1833-2016, 2016b.

Zhang, F., Peng, J., Chen, L., Collins, D., Li, Y., Jiang, S., Liu, J., Zhang, R.: The effect of Black carbon aging from NO2 oxidation of SO2 on its morphology, optical and hygroscopic properties, Environ. Res., 212, 113238, https://doi.org/10.1016/j.envres.2022.113238, 2022.

Zhao, G., Tan, T., Hu, S., Du, Z., Shang, D., Wu, Z., Guo, S., Zheng, J., Zhu, W., Li, M., Zeng, L., and Hu, M.: Mixing state of black carbon at different atmospheres in north and southwest China, Atmos. Chem. Phys., 22, 10861–10873, https://doi.org/10.5194/acp-22-10861-2022, 2022.

Zhang, F., Ren, J., Fan, T., Chen, L., Xu, W., Sun, Y., et al.: Significantly enhanced aerosol CCN activity and number, J. Geophys. Res.-Atmos., 124, 14102–14113, https://doi.org/10.1029/2019jd031457, 2019.

Zdanovskii, A.: New methods for calculating solubilities of electrolytes in multicomponent systems, Zh. Fiz. Khim.C, 22, 1475– 1485, 1948.

Zhang, R., Wang, G., Guo, S., Zamora, M. L., Ying, Q., Lin, Y.: Formation of urban fine particulate matter, Chemical Reviews, 115(10), 3803–3855, https://doi.org/10.1021/acs.chemrev.5b00067, 2015.

Zhang, Y., Zhang, Q., Yao, Z., Li, H.: Particle Size and Mixing State of Freshly Emitted

927 Black Carbon from Different Combustion Sources in China, Environ. Sci. Technol.,
928 54(13): p. 7766-7774, https://doi.org/10.1021/acs.est.9b07373, 2020b.